expression (Fig. 12A). It was notable that in medium containing 5 mM Pi, myogenesis was not inhibited and the C2C12 cells differentiated into myotubes, while the expression Runx2 was augmented (Fig. 12B). Further observation revealed that myogenin and Runx2 did not colocalize in the nuclei of myotubes, rather, Runx2 was localized in the cytoplasm. This finding suggests that Runx2 is inactive in myogenic cells, as it has been reported that Runx2 activity is regulated by translocation between the nucleus and cytoplasm (Zaidi et al., 2001). Upregulation of Runx2 expression was observed by Western blotting not only when the C2C12 cells were cultured under high-Pi conditions, but also when cultured in the presence of calcium deposits, which were generated by the addition of sodium phosphate and calcium chloride to the medium (Fig. 12C). Osteocalcin, another osteogenic marker which is a secreted protein whose expression is regulated by Runx2, was also examined (Fig 12D). RT-PCR was performed with RNA samples prepared from C2C12 cells cultured under the various Pi concentrations for four days. Osteocalcin expression was undetectable when the cells were cultured with 1 mM Pi, but increased with the elevation of the Pi concentration. We also measured calcium deposition in C2C12 cells cultured under the various Pi concentrations and found that although the cells did not deposit calcium under normal Pi conditions, cells cultured in medium containing 3 mM Pi or higher deposited calcium (alizarin red S-positive cells; Fig. 12E). The amount of calcium deposits increased significantly at higher Pi concentrations.

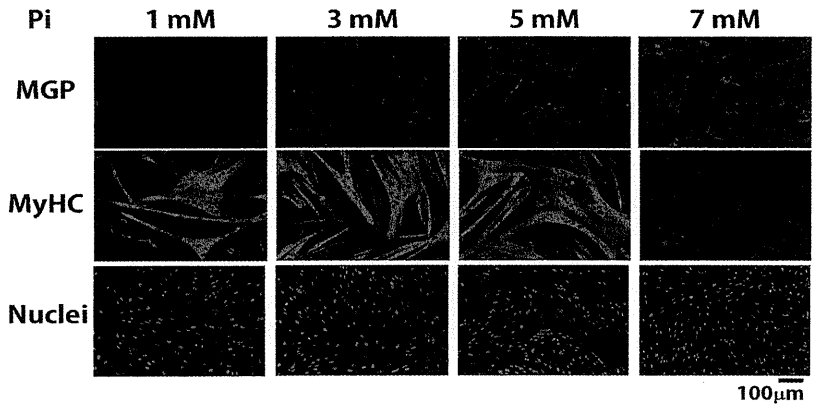

Fig. 11. Immunocytochemistry of C2C12 cells cultured under various Pi concentrations. Cells were immunostained for MyHC (green), MGP (red), and nuclei (blue).

8.2 Pi-induced calcification in primary cultures of skeletal muscle cells

Cells isolated from mdx skeletal muscle tissue were cultured in normal Pi (1.3 mM) to high-Pi (5 mM) medium to study the effects of Pi in primary culture cells. The cells formed myotubes when cultured in normal medium, whereas myotube formation was strongly inhibited under high-Pi conditions. The results of both alizarin red S and von Kossa staining revealed that numerous calcium deposits were present in cells after ten days of culture in high-Pi medium, but none detected in cells cultured in normal medium (Fig. 13). Therefore, Pi induces osteogenesis in myoblasts, resulting in calcification while inhibiting myogenesis. We conclude that the calcification of skeletal muscle is mainly due to the elevation of intracellular Pi levels.

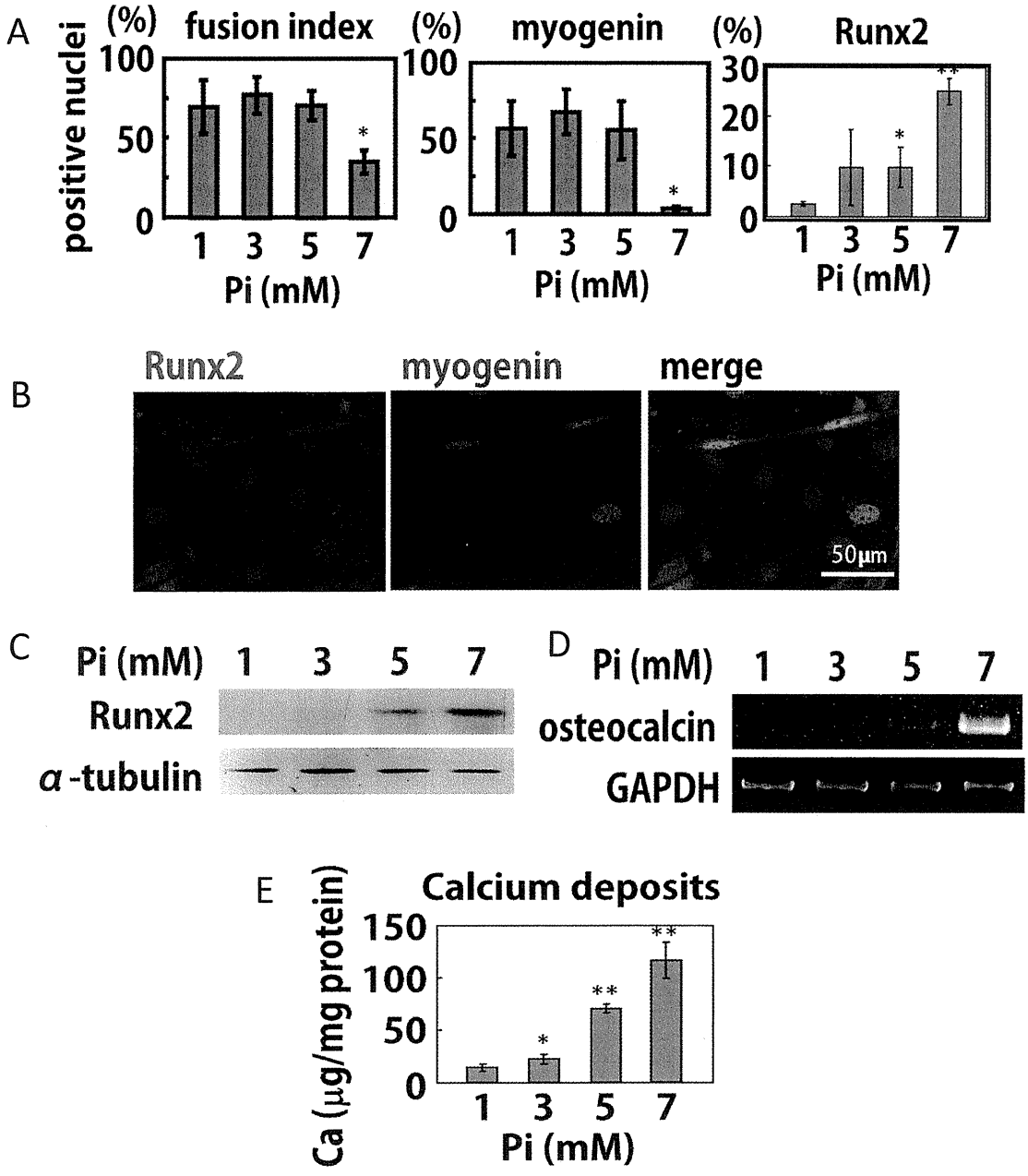

Fig. 12. Immunocytochemistry and RT-PCR of C2C12 cells cultured under various Pi concentrations (1, 3, 5, and 7 m). (A) The fusion index, myogenin expression, and expression of Runx2 were quantified. The fusion index and ratio of nuclei expressing myogenin decreased, while the ratio of Runx2-expressing nuclei increased with increasing Pi concentration. (B) Close observation of cells cultured in medium containing 5 mM Pi by staining with Hoechst 33258 to show the nuclei, or immunostained for myogenin or Runx2. (C) Western blotting of C2C12 cells cultured under increased Pi or Ca concentrations. (D) RT-PCR for osteocalcin in C2C12 cells cultured under various Pi concentrations. (E) Quantification of calcium deposites generated by C2C12 cells cultured under various Pi concentrations. (*: $p<0.05$; **: $p<0.01$).

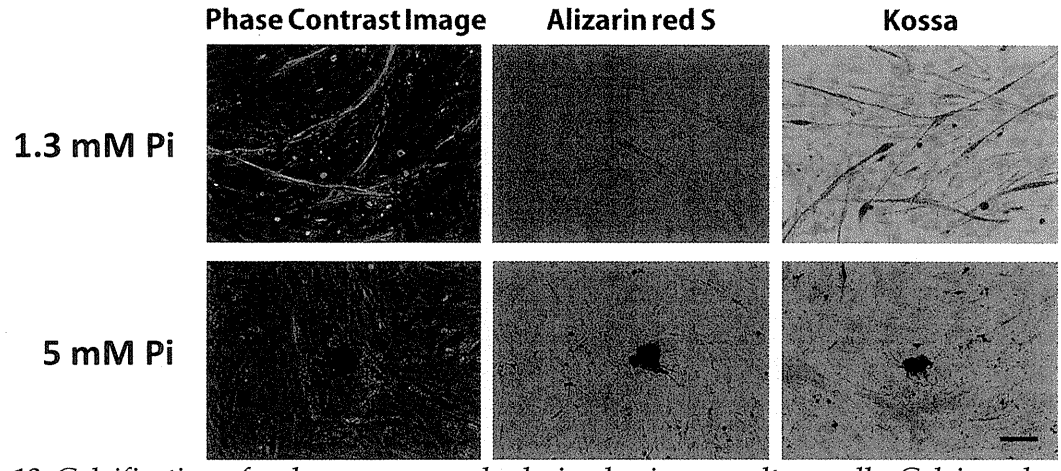

Fig. 13. Calcification of mdx mouse muscle-derived primary culture cells. Calcium deposits were stained red or black with alizarin red S and von Kossa staining, respectively. No calcification was observed when cells were cultured in normal medium containing 1.3 mM Pi. The von Kossa-stained samples were counterstained with nuclear fast red, and myotubes appear pink. The bar represents 100μm.

9. Conclusion

In this study, we reviewed the mechanisms underlying calcification in skeletal muscle cells following the elevation of intracellular Pi concentrations and revealed the effects of dietary phosphate intake on ectopic calcification in mdx mice. Both *in vivo* and *in vitro*, high-Pi conditions lead to the precipitation of calcium in mdx mice. We have demonstrated that the presence of ectopic calcification in skeletal muscle exacerbates the impaired muscle function of mdx mice, which represents a novel finding. The main goal of our studies is to understand the effects and efficacy of nutritional components on muscular dystrophy as a prior therapy. The effects of dietary phosphate intake on muscle pathology and kidney function need to further elucidated in future studies. Furthermore, the therapeutic potential of nutrition, particularly phosphate intake, should be considered when treating patients with DMD.

10. Acknowledgement

This work has been supported by Health and Labour Sciences Research Grant (19A-020) for Research on Psychiatric and Neurological Diseases and Mental Health, Intramural Research Grant(23-5) for Neurological and Psychiatric Disorders of NCNP and a Research Grant for Nervous and Mental Disorders [20B-13] from the Ministry of Health, Labour and Welfare, Japan.

11. References

Asakura, A.; Komaki, M. & Rudnicki, M. (2001). Muscle Satellite Cells are Multipotential Stem Cells that Exhibit Myogenic, Osteogenic, and Adipogenic Differentiation. Differentiation, Vol.68, pp.245-253.

Burbach, J. (1987). Ultrastructure of Cardiocyte Degeneration and Myocardial Calcification in the Dystrophic Hamster. *The American Journal of Anatomy*, Vol.179, pp.291-307.

Calvo, M. (1994). The Effects of High Phosphoru Intake on Calcium Homeostasis. *Advances in Nutritional Researches*, Vol.9, pp.183-207.

Costas, J.; Nye, D.; Henley, J. & Plochocki, J. (2010). Voluntary Exercise Induces Structural Remodeling in the Hearts of Dystrophin-deficient Mice. *Muscle Nerve*, Vol.42, pp.881-885.

Coulton, G.; Morgan, J.; Partridge, T. & Sloper, J. (1988). The mdx Mouse Skeletal Muscle Myopathy: I. A Histological, Morphometric and Biochemical Investigation. *Neuropathology and Applies Neurobiology*, Vol.14, pp.53-70.

Dingerkus, G. & Uhler, L. (1977). Enzyme Clearing of Alcian Blue Stained Whole Small Vertebrates for Demonstration of Cartilage. *Biotechnic & Histochemistry*, Vol.52, pp.229-232.

Dorchies, O.; Wagner, S.; Vuadens, O.; Waldhauser, K.; Buetler, T.; Kucera, P. & Ruegg, U. (2006). Green Tea Extract and Its Major Polyphenol(-)-epigallocatechin Gallate Improve Muscle Function in a Mouse Model of Duchenne Muscular Dystrophy. *American Journal of Physiology. Cell Physiology*, Vol.290, pp.616-625.

Draper, H. & Bell, R. (1979). Nutrition and Osteoporosis. *Advances in Nutritional Researches*, Vol.145, pp.389-391.

El-Abbadi, M.; Pai, A.; Leaf, E.; Yang, H.; Bartley, B.; Quan, K.; Ingalls, C.; Liao, H. & Giachelli, C. (2009). Phosphate Feeding Induces Arterial Medial Calcification in Uremic Mice: Role of Serum Phosphorus, Fibroblast Growth Factor-23, and Osteopontin. *Kidney International*, Vol.75, pp.1297-1307.

Elsherif, L.; Huang, M.; Shai, S.; Yang, Y.; Li, R.; Chun, J.; Mekany, M.; Chu, A.; Kaufman, S. & Ross, R. (2008). Combined Deficiency of Dystrophin and β1 Integrin in Cardiac Myocyte Causes Myocardial Dysfunction, Fibrosis and Calcification. *Circulation Research*, Vol.102, pp.1109-1117.

Gaschen, F.; Hoffman, E.; Gorospe, J.; Uhl, E.; Senior, D.; Cardinet, G. & Pearce, L. (1992). Dystrophin Deficiency Causes Lethal Muscle Hypertrophy in Cats. *Journal of the Neurological Sciences*, Vol.110, pp.149-159.

Giachelli, C. (2009). The Emerging Role of Phosphate in Vascular Calcification. Kidney International, V0l75, pp.890-897.

Hu, M.; Kuro-o,M. & Moe, O. (2010). Klotho and Kidney Disease. *Journal of Nephrology*, Vol.16, pp.136-144.

Kendrick, J.; Kestenbaum, B. & Chonchol, M. (2011). Phosphate and Cardiovascular Disease. *Advances in Chronic Kidney Disease*, Vol.18, pp.113-119.

Khan, M. (1993). Corticosteroid Therapy in Duchenne Muscular Dystrophy. *Journal of the Neurological Sciences*, V0l.120, pp.8-14.

Kikkawa, M.; Ohno, T.; Nagata, Y.; Shiozuka, M.; Kogure, T. & Matsuda, R. (2009). Ectopic Calcification is Caused by Elevated Levels of Serum Inorganic Phosphate in Mdx Mice. *Cell Structure and Function*, Vol.34, pp.77-88.

Korff, S.; Riechert, N.; Schoensiegel, F.; Weichenhan, D.; Autschbach, F.; Katus, H. & Ivandic, B. (2006). Calcification of Myocardial Necrosis is Common in Mice. *Virchows Archiv*, Vol.448, pp.630-638.

Kuro-o. (2010). Overview of the FGF-23-Klotho Axis. *Pediatric Nephrology*, Vol.25, pp.583-590.

Kuro-o, M.; Matsumura, Y.; Aizawa, H.; Kawaguchi, H.; Suga, T.; Utsugi, T.; Ohyama, Y.; Kurabayashi, M.; Kaname, T.; Kume, E.; Iwasaki, H.; Iida, A.; Shiraki-Iida, T.; Nishikawa, S.; Nagai, R. & Nabeshima, Y. (1997). Mutation of the Mouse *Klotho* Gene Leads to a Syndrome Resembling Ageing. *Nature*, Vol.309, pp.45-51.

Liu, J.; Okamura, C.; Bogan, D.; Bogan, J.; Childers, M. & Kornegay. J. (2004). Effects of Prednisone in Canine Muscular Dystrophy. *Muscle Nerve*, Vol.30, pp.767-773.

Lutwak, L. (1975). Metabolic and Biochemical Considerations of Bone. *Annals of Clinical and Laboratory Science*, Vol.5, pp.185-194.

Matsuda, R.; Nishikawa, A. & Tanaka, H. (1995). Visualization of Dystrophic Muscle Fibers in Mdx Mouse by Vital Staining with Evans Blue: Evidence of Apoptosis in Dystrophin-Deficient Muscle. *Journal of Biochemistry*, Vol.118, pp.959-964.

McLeod, M. (1980). Differential Staining of Cartilage and Bone in Whole Mouse Fetuses by Alcian Blue and Alizarin Red S. *Teratology*, Vol.22, pp.229-301.

Morishita, K.; Shirai, A.; Kubota, M.; Katakura, Y.; Nabeshima, Y.; Takeshige, K. & Kamiya, T. (2010). The Progression of Aging in *Klotho* Mutant Mice Can Be Modified by Dietary Phosphorus and Zinc. *The Journal of Nutrition*, Vol.131, pp.3182-3188.

Nguyen, F.; Cherel, L.; Guigand, I.; Goubault-Leroux & Myers, M. (2002). Muscle Lesions Associated with Dystrophin Deficiency in Neonatal Golden Retriver Puppies. *Journal of Comparative Pathology*, Vol.126, pp.100-108.

Quinlan, J.; Johnson, S.; McKee, M. & Lyden, S. (1992). Twitch and Tetanus in mdx Mouse Muscle. *Muscle Nerve*, Vol.15, pp.837-842.

Razzaque, M.; Sitara, D.; Taguchi, T.; St-Arnaud, R. & Lanske, B. (2006). Premature Aging-like Phenotype in Fibroblast Growth Factor 23 Null Mice is a Vitamin D Mediated Process. *The FASEB Journal*, Vol.20, pp.720-722.

Vercherat, C.; Chung, T.; Yalcin, S.; Gulbagci, N.; Gopinadhan, S.; Ghaffari, S. & Taneja, R. (2009). Stra13 Regulates Oxidative Stress Mediated Skeletal Muscle Degeneration. *Human Molecular Genetics*, Vol.18, pp.4304-4316.

Verma, M.; Asakura, Y.; Hirai, H.; Watanabe, S.; Tastad, C.; Fong, G.; Ema, M.; Call, J.; Lowe, D. & Asakura, A. (2010). *Fit-1* Haploinsufficiency Ameliorates Muscular Dystrophy Phenotype by Developmentally Increased Vasculature in Mdx Mice. *Human Molecular Genetics*, Vol.19, pp.4145-4159.

Wada, M.; Inagawa-Ogashiwa, M.; Shimizu, S.; Yasumoto, S. & Hashimoto, N. (2002). Generation of Different Fates from Multipotent Muscle Stem Cells. *Development*, Vol.129, pp.2987-2995.

Webb, G. & Byrd, R. (1994). Simultaneous Differential Staining of Cartilage and Bone in Rodent Fetuses: an Alcian Blue and Alizarin Red S Procedure Without Glacial Acetic Acid. *Biotechnic and Histochemistry*, Vol.64, pp.181-185.

Wong, B. & Christopher, C. (2002). Corticosteroids in Duchenne Muscular Dystrophy: a Reappraisal. *Journal of Child Neurology*, Vol.17, pp.183-190.

Zaidi, S.; Javed, A.; Choi, J.; van Wijnen, A.; Stein, J.; Lian, J. & Stein, G. (2001). A Specific Targeting Signal Directs Runx2/Cbfa1 to Subnuclear Domains and Contributes to Transactivation of the Osteocalcin Gene. *Journal of Cell Sciences*, Vol.114, pp.3093-3102.

Zhang, W.; Hove, M.; Schneider, J.; Stuckey, D.; Sebag-Montefiore, L.; Bia, B.; Radda, G.; Davis, K.; Neubauer, S. & Clarke, K. (2008). Abnormal Cardiac Morphology, Function and Energy Metabolism in the Dystrophic mdx Mouse: An MRI and MRS Study. *Journal of Molecular and Cellular Cardiology*, Vol.45, pp.754-760.

ACS Medicinal Chemistry Letters

Letter

pubs.acs.org/acsmedchemlett

Negamycin Analogue with Readthrough-Promoting Activity as a Potential Drug Candidate for Duchenne Muscular Dystrophy

Akihiro Taguchi,[†] Shigenobu Nishiguchi,[‡] Masataka Shiozuka,[§] Takao Nomoto,[†] Mayuko Ina,[†] Shouta Nojima,[†] Ryoichi Matsuda,[§] Yoshiaki Nonomura,[§,∥] Yoshiaki Kiso,[‡] Yuri Yamazaki,[†] Fumika Yakushiji,[†] and Yoshio Hayashi*[,†]

[†]Department of Medicinal Chemistry, Tokyo University of Pharmacy and Life Sciences, Hachioji, Tokyo 192-0392, Japan

[‡]Department of Medicinal Chemistry, Kyoto Pharmaceutical University, Yamashina-ku, Kyoto 607-8412, Japan

[§]Department of Life Sciences, Graduate School of Arts and Sciences, The University of Tokyo, Komaba, Tokyo 153-8902, Japan

[∥]Institute of Microbial Chemistry, Shinagawa-ku, Tokyo 141-0021, Japan

Supporting Information

ABSTRACT: A series of (+)-negamycin **1** analogues were synthesized, and their readthrough-promoting activity was evaluated for nonsense mutations in Duchenne muscular dystrophy (DMD). A structure–activity relationship study indicated that **11b** was the most potent drug candidate. Immunohistochemical analyses suggested that treatment with **11b** restored dystrophin expression in *mdx* mice, a DMD mouse model. Furthermore, **11b** decreased serum creatine kinase (CK) levels, an indicator of muscle fiber destruction. Most importantly, **11b** demonstrated lower toxicity than **1**, and thus, it could be a useful candidate for long-term treatment of DMD.

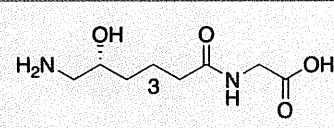

11b

KEYWORDS: *Negamycin, readthrough-promoting activity, Duchenne muscular dystrophy, nonsense mutations, hydrazino dipeptide, genetic disease*

Duchenne muscular dystrophy (DMD), characterized by progressive muscle degeneration, is one of the most common hereditary disorders, affecting approximately 1 in 3500 live male births.[1] This disorder is caused by mutations in the DMD gene, located on the X-chromosome. The DMD gene encodes the protein dystrophin, which plays a crucial role linking the intracellular cytoskeleton and the extracellular matrix via the dystrophin-associated protein complex (DAPC). The loss of dystrophin function causes destabilization of the DAPC, which results in the breakdown of muscle fibers, loss of membrane integrity, and difficulty in walking and breathing, and it ultimately leads to death. Nonsense mutations, which lead to premature termination codons (PTCs) in the reading frame of the DMD gene, are responsible for up to 20% of DMD cases. The nonsense mutations yield truncated dystrophin proteins, which have no valuable biological function.[2] Presently, although the molecular basis for the disease is clear, there is no cure for DMD.[3] The only available treatment is glucocorticoid therapy, which can prolong ambulation and reduce the incidence of severe scoliosis, although it is limited to relatively short-term treatments due to severe side effects.[4−6]

Recently, a unique therapeutic strategy, so-called "read-through drugs", was proposed to target genetic diseases caused by nonsense mutations.[7] These drugs promote a translational "skip" of PTCs, but not of normal termination codons, resulting in the production of full-length proteins. Specifically, gentamicin, an aminoglycoside antibiotic, was reported to promote the readthrough of disease-causing PTCs in mammalian cells. Furthermore, its treatment partially restored dystrophin expression in skeletal and cardiac muscles of *mdx* mice, an animal model of DMD with a nonsense mutation in the dystrophin gene. In spite of these positive results, long-term administration of gentamicin is not recommended, due to its severe side-effects including ototoxicity[8] and nephrotoxicity.[9] Small molecules possessing readthrough-promoting activity have also been described for DMD treatment, including aminoglycosides,[10] RTC compounds,[11] and an oxadiazole derivative, ataluren (PTC-124, phase IIB).[12]

In the same vein, Arakawa et al.[13] reported that the dipeptidic antibiotic (+)-negamycin (**1**, [2-(3,6-diamino-5-hydroxyhexanoyl)-1-methylhydrazino]acetic acid, Figure 1)[14] also induced

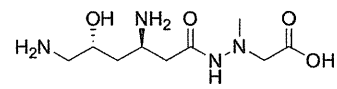

Figure 1. Structure of (+)-negamycin **1**.

the readthrough of PTCs in both a prokaryotic translational system[15] and *mdx* mice.[13] Therefore, **1** has been recognized as a potential therapeutic agent for diseases caused by nonsense mutations. Here, we designed and synthesized a series of negamycin analogues, and their biological activity was evaluated using a transgenic mouse strain, READ (readthrough evaluation and assessment by dual reporter),[16] which expresses a dual-reporter gene segmentalized with a PTC. Once the most potent

Received: October 19, 2011
Accepted: January 2, 2012
Published: January 2, 2012

Table 1. Readthrough-Promoting and Antimicrobial Activities of Synthetic Negamycin Analogues

Compound	Structure	Yield (%) [a]	Readthrough activity [c]	Antimicrobial activity [d]
Gentamicin	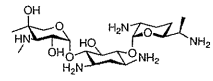	NA [b]	1.00 ± 0.24	NT [e]
1 (+)-negamycin	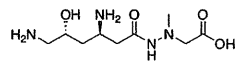	NA [b]	1.00 ± 0.25	32/128/2/32/8
6	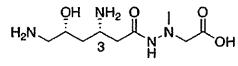	32	1.01 ± 0.16	>50/>50/25/>50/50
11a	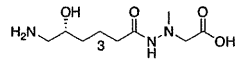	27	0.83 ± 0.13	–
11b	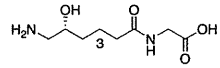	27	1.36 ± 0.14	–
11c	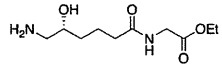	43	0.81 ± 0.11	–
11d	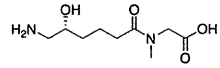	44	0.92 ± 0.09	NT [e]
11e	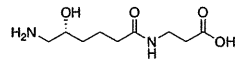	24	< 0.8	–
11f	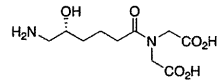	13	< 0.8	NT [e]
14	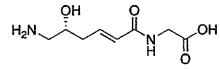	24	< 0.8	–

[a]Synthetic yields were calculated from intermediates **3** or **7** for analogues **6** or **11a–f** and **14**, respectively. [b]NA; not applicable, see ref 18. [c]Relative *in vivo* readthrough-promoting activity, which is expressed as a ratio compared to gentamicin. Samples were subcutaneously injected at the abdominal region of the READ mouse with a dosage of 0.1 mg/day/20 g body-weight for 7 days. Data are mean ± SD (n = 4). [d]The antimicrobial activity (MIC) against several microorganisms (*Staphylococcus aureus* FDA 209P/*Bacilus subtilis* NRRL B-558/*Escherichia coli* BEM11/*Shigella dysenteriae* J S11910/*Pseudomonas aeruginosa* A3, respectively). "– " denotes >128 μg/mL (MIC). See ref 24. [e]NT: not tested.

11b had been identified (Table 1), we used *mdx* mice to assess the effect on dystrophin expression, serum creatine kinase levels,[17] which are a clinical indicator of DMD, and general toxicity. We found that **11b** performed better than **1**, with markedly reduced toxicity, thus making it a promising therapeutic candidate.

(+)-Negamycin **1** was first isolated in 1970 from a microorganism closely related to *Streptomyces purpeofuscus*.[14] In an attempt to synthesize chiral **1**, we developed shortened, highly efficient synthetic routes.[18,19] Using one of these routes as a starting point,[19] here, we synthesized a series of analogues. Briefly, for the synthesis of analogue **6** (Scheme 1A), intermediate **3** was prepared from the commercially available ester **2** over 7 steps.[19] Then, **3** was converted to the *N*-protected *tert*-butyl ester **4** as a single diastereomer (diastereomeric excess (de) >99%) over 3 steps using Node's asymmetric Michael addition,[20] removal of the chiral auxiliary,[21] and protection of the inserted 3-amino group. The obtained intermediate **4** was then efficiently converted to the acid form by a microwave-assisted saponification, and it was subsequently coupled with a hydrazino ester using an EDC-HOBt (EDC, 1-ethyl-3-(3-dimethylaminopropyl)carbodiimide; HOBt, 1-hydroxybenzotriazole) method[22] to yield **5**. Deprotection of **5** with 4 M HCl/dioxane and purification by ion exchange chromatography afforded **6** (specific rotation: found $[\alpha]_D^{26.4}$ +14.0 (c 0.94, H_2O), literature data[23] $[\alpha]_D^{22.0}$ +8.5 (c 0.70, H_2O)).

Next, analogues **11a–f** were synthesized (Scheme 1B). Weinreb amide **7**[19] was prepared from **2** over six steps, and then it was reduced with diisobutylaluminium hydride (DIBAL-H) to the corresponding aldehyde, directly followed by treatment with (benzyloxycarbonylmethylene)triphenylphosphorane in THF under reflux conditions. After purification by flash chromatography on silica (Silica Gel 60N, KANTO CHEMICAL), we obtained **8** in 69% yield over two steps. After **8** was treated with Pd/C under a H_2 atmosphere, the resultant **9** was coupled with various amino acid *tert*-butyl esters or a hydrazinoacid *tert*-butyl ester[18] using an EDC-HOBt method to obtain **10a–f**. Deprotection of **10a–f** with 4 M HCl/dioxane and purification by reversed-phase HPLC afforded **11a–f** with 30–96% yield.

In the synthesis of analogue **14** (Scheme 1C), **7** was converted to the intermediate **12** by a procedure similar to that employed for **8** (Scheme 1B). Then, **12** was converted to the acid form by saponification and subsequently coupled with HCl·H-Gly-O*t*-Bu using an EDC-HOBt method to yield **13**. Deprotection of **13** with 4 M HCl/dioxane and purification by reversed-phase HPLC afforded **14** with 85% yield. The purity of each synthesized analogue for biological evaluation was over 95%.

To evaluate the readthrough-promoting activity, we adapted an *in vivo* dual-reporter gene expression system using READ mice.[16] This system encodes β-galactosidase and luciferase genes connected with a PTC (see the Supporting Information). β-Galactosidase activity is present constitutively, but luciferase

dx.doi.org/10.1021/ml200245t | *ACS Med. Chem. Lett.* 2012, 3, 118–122

Scheme 1. Synthesis of Analogue 6[a]

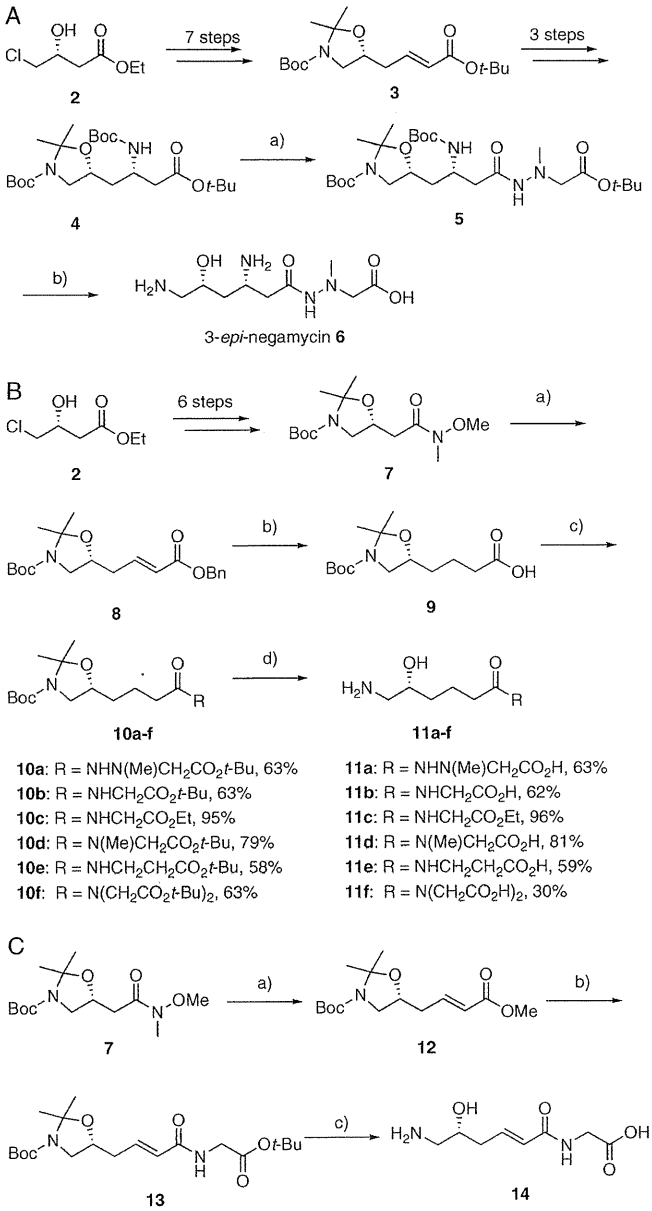

[a]Reagents and conditions: (A) Synthesis of **6**: (a) (i) KOH, MeOH, microwave (300 W), 100 °C, 10 min; (ii) PTSA·H_2N–N(Me)-CH_2CO_2t-Bu, HOBt·H_2O, Et_3N, EDC·HCl, CH_2Cl_2, rt, 4 h, 62% (2 steps); (b) (i) 4 M HCl/dioxane, rt, 1 h; (ii) ion exchange chromatography, 98%. (B) Synthesis of **11a–f**: (a) (i) DIBAL-H, toluene, −78 °C, 2 h; (ii) Ph_3P = $CHCO_2Bn$, THF, reflux, overnight, 69% (2 steps); (b) Pd/C, H_2, MeOH, rt, 1.5 h, quant; (c) amino acid *t*-Bu esters or hydrazinoacid *t*-Bu ester, HOBt·H_2O, Et_3N, EDC·HCl, DMF, rt, 3 h to overnight, 58–95%; (d) (i) 4 M HCl/dioxane, rt, 1 h; (ii) reversed-phase HPLC, 30–96%. (C) Synthesis of **14**: (a) (i) DIBAL-H, toluene, −78 °C, 2 h; (ii) Ph_3P = $CHCO_2Me$, THF, reflux, overnight, 63% (2 steps); (b) (i) KOH, MeOH/H_2O (2:1), rt, 4 h; (ii) HCl·H-Gly-O*t*-Bu, HOBt·H_2O, Et_3N, EDC·HCl, DMF, rt, overnight, 44% (2 steps); (c) (i) 4 M HCl/dioxane, rt, 1 h; (ii) reversed-phase HPLC, 85%.

activity is only detected when readthrough occurs. Therefore, the activities of both enzymes in skeletal muscle were measured to calculate the activity ratio of luciferase to β-galactosidase after negamycin analogues (0.1 mg) were subcutaneously administered in the abdominal region of READ mice for 7 days. The antimicrobial activity was also measured.[24] The results of these biological evaluations are shown in Table 1.

Since synthetic **1** showed similar levels of readthrough-promoting activity to the extracted native **1** (data not shown) and gentamicin, we first evaluated the importance of stereochemistry at the 3-amino group. The (+)-3-*epi*-negamycin **6** exhibited equipotent activity to **1**, suggesting that the stereochemistry of the 3-amino group might not be important for the activity. Next, analogue **11a** with no 3-amino group was prepared (Table 1). However, complete removal of the amino group led to a decrease and a loss of the readthrough-promoting and antimicrobial activities, respectively. Thus, the presence, but not the stereochemistry, of the 3-amino group was important for both biological activities.

In striking contrast, however, we observed that when both the *N*-methyl and amino groups were omitted from **11a**, the corresponding glycine analogue **11b** was a potent promoter of readthrough activity, demonstrating a 1.4-fold increase in functionality as compared to the case of **1**. Importantly, **11b** also did not display antimicrobial activity, making it a more selective readthrough-promoting analogue than **1**. In other words, it means that the readthrough-promoting activity can be distinguished from the antimicrobial activity.

Encouraged by these results, we synthesized additional analogues based on the chemical structure of **11b**. However, both the ethyl ester analogue **11c** and the *N*-methyl glycine analogue **11d** demonstrated decreased activities. From these results, we inferred that the glycine residue with a free carboxylic acid was functionally important, a hypothesis that we confirmed using **11e** and **11f**. Moreover, **14**, with the unsaturated amide structure, did not show any significant activity.

To understand the biological effects in detail, the most active **11b** was chosen for further *in vivo* immunohistochemical and biochemical evaluations. Regarding the immunohistochemical evaluation, **11b** was subcutaneously injected in the abdominal region of *mdx* mice at a dosage of 1 mg in phosphate-buffered saline (PBS, 0.2 mL)/day/20 g body-weight for 4 weeks. Dystrophin expression was clearly observed in the skeletal muscle of wild-type B10 mice (Figure 2A), while *mdx* mice

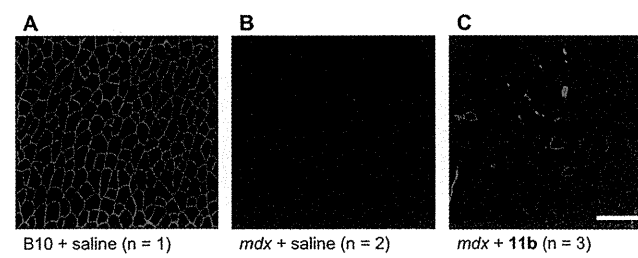

Figure 2. Dystrophin expression in skeletal muscles. Immunofluorescent staining of dystrophin in mouse muscle tissues was performed on 8 μm transverse cryosections.[12] (A) wild-type B10 mouse; (B) untreated *mdx* mouse; (C) **11b**-treated *mdx* mouse. Bar = 200 μm.

lacked this signal (Figure 2B). In contrast to these controls, dystrophin expression was only partially restored in the skeletal muscle of **11b**-treated *mdx* mice (Figure 2C). However, this result suggested that **11b** promotes PTC readthrough and is therefore a potential therapeutic candidate for DMD.

Regarding biochemical evaluation, we assessed levels of serum creatine kinase (CK)[17] in *mdx* mice treated subcutaneously with **11b** at a dosage of 1 mg in PBS (0.2 mL)/day/20

dx.doi.org/10.1021/ml200245t | ACS Med. Chem. Lett. 2012, 3, 118–122

g body-weight for 4 weeks. As controls, the CK level in a wild-type B10 mouse was very low, while levels in *mdx* mice were very high. A statistically significant reduction of serum CK levels in **11b**-treated *mdx* mice was observed in comparison to the case of the untreated controls (Figure 3A). This result

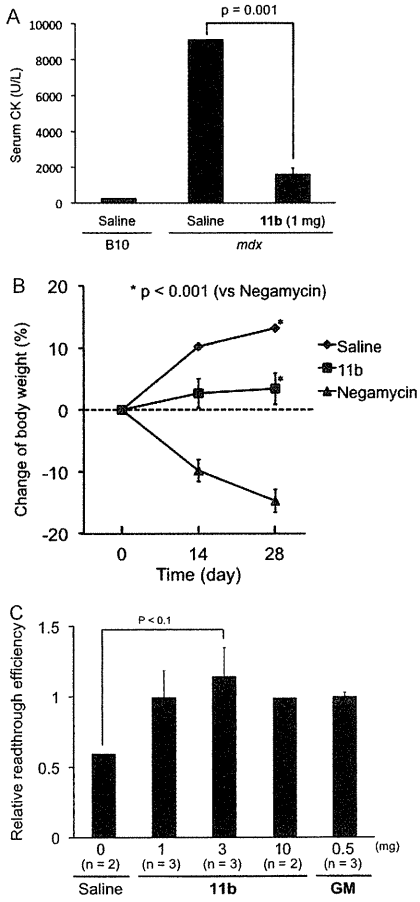

Figure 3. (A) Serum CK levels in *mdx* mice: wild-type B10 (n = 1); *mdx* (n = 2); **11b**-treated *mdx* (n = 3). (B) Effect of **11b** on the body-weight of *mdx* mice. The body-weight of **1**- and **11b**-treated mice (n = 4, 1 mg/day/20 g body-weight) over the course of 4 weeks was measured in comparison to that of saline-treated mice (n = 2) as a control. (C) Effects of the administration of high doses of **11b** on the readthrough-promoting activity in READ mice. P: Probability-value. Error bar indicates SD.

suggested that **11b** could enhance the strength of muscle fibers by increasing functional protein expression.

Next, we examined the acute *in vivo* toxicity of **11b** as compared to **1** by measuring the body-weight change of *mdx* mice for 4 weeks. Improving the *in vivo* toxicity profile of **1** was an important goal for the development of readthrough drugs based on the negamycin structure. As shown in Figure 3B, over the course of 4 weeks, the body-weight of saline-treated mice gradually increased, while that of **1**-treated mice (1 mg in 0.2 mL saline/day/20 g body-weight) markedly decreased. Conversely, the body-weight of **11b**-treated mice (1 mg in 0.2 mL saline/day/20 g body-weight) slowly increased during this time frame, indicating that **11b** exhibited a lower toxicity profile than **1**. We postulate that this lower toxicity is due to the absence of the hydrazine structure in **11b**. This improved toxicity profile strongly supports the potential of **11b** for the long-term treatment of DMD.

Finally, inspired by the low toxicity observed with **11b**, we tested the effects of high doses of **11b** on PTC readthrough-promoting activity. Accordingly, **11b**, or gentamicin or saline, as positive and negative controls, respectively, was administered subcutaneously in READ mice for 7 days. As shown in Figure 3C, the readthrough-promoting activity of **11b** was not dose-dependent at the levels tested. However, at a 3 mg dose, **11b** was more effective than gentamicin. For unknown reasons, there appeared to be a reduction in readthrough-promoting activity at the highest dosage of **11b**, an observation that we will pursue in the near future.

In summary, we have synthesized a series of (+)-negamycin analogues and evaluated their readthrough-promoting activity for DMD. On the basis of SAR studies, we identified **11b** as the most potent candidate. This analogue was then taken forward through immunohistochemical and biochemical studies, which demonstrated that treatment with **11b** restored some dystrophin expression in *mdx* mice and decreased their serum CK levels, indicating that the drug was protecting muscular tissues from collapse. Most importantly, **11b** was shown to have a lower toxicity profile than **1**, which might be useful for the long-term treatment of DMD. Further SAR studies to develop more efficient derivatives are under investigation.

■ ASSOCIATED CONTENT

Supporting Information

Synthetic procedures, characterization of new products, biological assay protocols, and NMR data. This material is available free of charge via the Internet at http://pubs.acs.org.

■ AUTHOR INFORMATION

Corresponding Author

*E-mail: yhayashi@toyaku.ac.jp. Telephone: +81-42-676-3275. Fax: +81-42-676-3275.

Funding Sources

This research was supported by an Intramural Research Grant (23-5) for Neurological and Psychiatric Disorders of NCNP, a Grant-in-Aid for Scientific Research (B) (No. 20390036) from MEXT (Ministry of Education, Culture, Sports, Science and Technology), the Ichiro Kanehara Foundation, Sasakawa Grants for Science Follows (to M.S.) partly, and a Health and Labor Sciences Research Grant for Research, Comprehensive Research on Disability Health and Welfare (19A-020 and H22-016) from the Ministry of Health, Labor and Welfare, Japan.

Notes

The authors declare no competing financial interest.

■ ACKNOWLEDGMENTS

The authors thank Ms. Miyuki Hiroshima and Ms. Yumi Sakurai, Tokyo University of Pharmacy and Life Sciences, for technical assistance and Dr. Minoru Ozeki and Emeritus Professor Manabu Node, Kyoto Pharmaceutical University, for technical advice regarding the asymmetric Michael addition.

■ REFERENCES

(1) Nowak, K. J.; Davies, K. E. Duchenne muscular dystrophy and dystrophin: pathogenesis and opportunities for treatment. *EMBO Rep.* **2004**, *5*, 872–876.

(2) Malik, V.; Rodino-Klapac, L. R.; Viollet, L.; Mendell, J. R. Aminoglycoside-induced mutation suppression as a therapeutic

strategy for Duchenne muscular dystrophy. *Ther. Adv. Neurol. Disord.* **2010**, *3*, 379–389.

(3) Monaco, A. P.; Neve, R. L.; Colletti-Feener, C.; Bertelson, C. J.; Kurnit, D. M.; Kunkel, L. M. Isolation of candidate cDNAs for portions of the Duchenne muscular dystrophy gene. *Nature* **1986**, *323*, 646–650.

(4) Granchelli, J. A.; Pollina, C.; Hudecki, M. S. Pre-clinical screening of drugs using the *mdx* mouse. *Neuromuscular Disord.* **2000**, *10*, 235–239.

(5) Griggs, R. C.; Moxley, R. T. III; Mendell, J. R.; Fenichel, G. M.; Brooke, M. H.; Pestronk, A.; Miller, J. P.; Cwik, V. A.; Pandya, S.; Robinson, J. Duchenne dystrophy: randomized, controlled trial of prednisone and azathioprine. *Neurology* **1993**, *43*, 520–527.

(6) Khurana, T. S.; Davies, K. E. Pharmacological strategies for muscular dystrophy. *Nat. Rev. Drug Discovery* **2003**, *2*, 379–390.

(7) Barton-Davis, E. R.; Cordier, L.; Shoutourma, D. I.; Leland, S. E.; Sweeney, H. L. Aminoglycoside antibiotics restore dystrophin function to skeletal muscles of *mdx* mice. *J. Clin. Invest.* **1999**, *104*, 375–381.

(8) Hutchin, T.; Cortopassi, G. Proposed molecular and cellular mechanism for aminoglycoside ototoxicity. *Antimicrob. Agents Chemother.* **1994**, *38*, 2517–2520.

(9) Mingeot-Leclercq, M. P.; Tulkens, P. M. Aminoglycosides: Nephrotoxicity. *Antimicrob. Agents Chemother.* **1999**, *43*, 1003–1012.

(10) Nudleman, I.; Rebibo-Sabbah, A.; Cherniavsky, M.; Belakhov, V.; Hainrichson, M.; Chen, F.; Schacht, J.; Pilch, D. S.; Ben-Yosef, T.; Baasov, T. Development of novel aminoglycoside (NB54) with reduced toxicity and enhanced suppression of disease-causing premature stop mutations. *J. Med. Chem.* **2009**, *52*, 2836–2845.

(11) Du, L.; Damoiseaux, R.; Nahas, S.; Gao, K.; Hu, H.; Pollard, J. M.; Goldstine, J.; Jung, M. E.; Henning, S. M.; Bertoni, C.; Gatti, R. A. Nonaminoglycoside compounds induce readthrough of nonsense mutations. *J. Exp. Med.* **2009**, *206*, 2285–2297.

(12) Welch, E. M.; Barton, E. R.; Zhuo, J.; Tomizawa, Y.; Friesen, W. J.; Trifillis, P.; Paushkin, S.; Patel, M.; Trotta, C. R.; Hwang, S.; Wilde, R. G.; Karp, G.; Takasugi, J.; Chen, G.; Jones, S.; Ren, H.; Moon, Y.; Corson, D.; Turpoff, A. A.; Campbell, J. A.; Conn, M. M.; Khan, A.; Almstead, N. G.; Hedrick, J.; Mollin, A.; Risher, N.; Weetall, M.; Yeh, S.; Branstrom, A. A.; Colacino, J. M.; Babiak, J.; Ju, W. D.; Hirawat, S.; Northcutt, V. J.; Miller, L. L.; Spatrick, P.; He, F.; Kawana, M.; Feng, H.; Jacobson, A.; Peltz, S. W.; Sweeney, H. L. PTC124 targets genetic disorders caused by nonsense mutations. *Nature* **2007**, *447*, 87–91.

(13) Arakawa, M.; Shiozuka, M.; Nakayama, Y.; Hara, T.; Hamada, M.; Kondo, S.; Ikeda, D.; Takahashi, Y.; Nonomura, Y.; Sheykholeslami, K.; Kondo, K.; Kaga, K.; Kitamura, T.; Suzuki-Miyagoe, Y.; Takeda, S.; Matsuda, R. Negamycin restores dystrophin expression in skeletal and cardiac muscles of *mdx* mice. *J. Biochem.* **2003**, *134*, 751–758.

(14) Hamada, M.; Takeuchi, T.; Kondo, S.; Ikeda, Y.; Naganawa, H.; Maeda, K.; Okami, Y.; Umezawa, H. A new antibiotic, negamycin. *J. Antibiot.* **1970**, *23*, 170–171.

(15) Uehara, Y.; Hori, M.; Umezawa, H. Negamycin inhibits termination of protein synthesis directed by phage f2 RNA in vitro. *Biochim. Biophys. Acta* **1974**, *374*, 82–95.

(16) Shiozuka, M.; Wagatsuma, A.; Kawamoto, T.; Sasaki, H.; Shimada, K.; Takahashi, Y.; Nonomura, Y.; Matsuda, R. Transdermal delivery of a readthrough-inducing drug: a new approach of gentamicin administration for the treatment of nonsense mutation-mediated disorders. *J. Biochem.* **2010**, *147*, 463–470.

(17) Ebashi, S.; Toyokuma, Y.; Momoi, H.; Sugita, H. High creatine phosphokinase activity of sera of progressive muscular dystrophy. *J. Biochem.* **1959**, *46*, 103–104.

(18) Hayashi, Y.; Regnier, T.; Nishiguchi, S.; Magne, O. S.; Hashimoto, D.; Hasegawa, J.; Katoh, T.; Kajimoto, T.; Shiozuka, M.; Matsuda, R.; Node, M.; Kiso, Y. Efficient total synthesis of (+)-negamycin, a potential chemotherapeutic agent for genetic diseases. *Chem. Commun.* **2008**, 2379–2381.

(19) Nishiguchi, S.; Magne, O. S.; Taguchi, A.; Regnier, T.; Kajimoto, T.; Node, M.; Yamazaki, Y.; Yakushiji, F.; Kiso, Y.; Hayashi, Y. Total synthesis of (+)-negamycin and its 5-*epi*-derivative. *Tetrahedron* **2010**, *66*, 314–320.

(20) Node, M.; Hashimoto, D.; Katoh, T.; Ochi, S.; Ozeki, M.; Watanabe, T.; Kajimoto, T. Asymmetric Michael addition of a recyclable chiral amine: inversion of stereoselectivity caused by the difference of ethereal solvents. *Org. Lett.* **2008**, *10*, 2653–2656.

(21) Katoh, T.; Watanabe, T.; Nishitani, M.; Ozeki, M.; Kajimoto, T.; Node, M. Selective C-N bond oxidation: demethylation of *N*-methyl groups in *N*-arylmethyl-*N*- methyl-α-amino esters utilizing *N*-iodosuccinimide (NIS). *Tetrahedron Lett.* **2008**, *49*, 598–600.

(22) Konig, W.; Geiger, R. A. A new method for synthesis of peptides: activation of the carboxyl group with dicyclohexylcarbodiimide using 1-hydroxybenzotriazoles as additives. *Chem. Ber.* **1970**, *103*, 788–798.

(23) Davies, S. G.; Ichihara, O.; Robert, P. M.; Thomson, J. E. Asymmetric syntheses of (+)-negamycin, (+)-3-*epi*-negamycin and sperabillin C via lithium amide conjugate addition. *Tetrahedron* **2011**, *67*, 216–227.

(24) The antimicrobial activity (MIC) was measured with the routine screening system at the Institute of Microbial Chemistry (IMC), Tokyo, Japan, using the agar dilution streak method (2-fold dilution) in Mueller Hinton agar (Difco) at 37 °C for 18 h against 34 microorganisms.

Correlation of within-individual fluctuation of depressed mood with prefrontal cortex activity during verbal working memory task: optical topography study

Hiroki Sato,[a,*] Ryuta Aoki,[b,c,*] Takusige Katura,[a] Ryoichi Matsuda,[b] and Hideaki Koizumi[a]
[a]Hitachi, Ltd., Central Research Laboratory, 2520 Akanuma, Hatoyama, Saitama 350-0395, Japan
[b]The University of Tokyo, Graduate School of Arts and Sciences, 3-8-1 Komaba, Meguro-ku, Tokyo 153-8902, Japan
[c]Japan Society for the Promotion of Science, 8 Ichibancho, Chiyoda-ku, Tokyo 102-8472, Japan

Abstract. Previous studies showed that interindividual variations in mood state are associated with prefrontal cortex (PFC) activity. In this study, we focused on the depressed-mood state under natural circumstances and examined the relationship between within-individual changes over time in this mood state and PFC activity. We used optical topography (OT), a functional imaging technique based on near-infrared spectroscopy, to measure PFC activity for each participant in three experimental sessions repeated at 2-week intervals. In each session, the participants completed a self-report questionnaire of mood state and underwent OT measurement while performing verbal and spatial working memory (WM) tasks. The results showed that changes in the depressed-mood score between successive sessions were negatively correlated with those in the left PFC activation for the verbal WM task ($\rho = -0.56$, $p < 0.05$). In contrast, the PFC activation for the spatial WM task did not co-vary with participants' mood changes. We thus demonstrated that PFC activity during a verbal WM task varies depending on the participant's depressed mood state, independent of trait factors. This suggests that using optical topography to measure PFC activity during a verbal WM task can be used as a potential state marker for an individual's depressed mood state. [DOI: 10.1117/1.3662448]

Keywords: depressed mood; working memory; prefrontal cortex; near-infrared spectroscopy; optical topography; profile of mood states.

Paper 11243R received May 17, 2011; revised manuscript received Oct. 20, 2011; accepted for publication Oct. 25, 2011; published online Nov. 28, 2011.

1 Introduction

The relationship between mood and cognition, as well as the neural mechanisms supporting it, has long attracted researchers in psychology and neuroscience.[1,2] Behavioral experiments have shown that even mild variations in mood state influence various cognitive functions such as working memory (WM) and cognitive fluency.[1,3,4] Recent neuroimaging studies have implicated the prefrontal cortex (PFC) as one of the key regions that converges mood and cognition in the brain.[1,2] For instance, functional magnetic resonance imaging (fMRI) studies have reported that experimentally induced negative moods affect PFC activity during cognitive tasks such as WM and Stroop tasks.[5,6] In addition, near-infrared spectroscopy (NIRS) studies focusing on moods under natural circumstances indicate that people having a high level of fatigue or sleepiness showed decreased PFC activity in response to verbal fluency tasks.[7,8] However, little is known about how PFC activity during cognitive tasks and natural moods, which can vary across days or weeks, are coupled within individuals. Thus, tracking within-individual fluctuations in natural mood and PFC activity during cognitive tasks is necessary to deepen our knowledge about their relationship.

In our previous study, we used optical topography (OT), which is a noninvasive functional imaging-technique based on NIRS,[9–11] to show that a variation in the negative mood state across participants is correlated with their PFC activity for a verbal WM task.[12] OT measures hemodynamic responses in the cerebral cortex under near-natural situations (e.g., sitting position) and allows us to minimize mood modulation due to the experiment itself. In the previous study, the participants' natural moods were assessed by using the Profile of Mood States (POMS), a self-reporting questionnaire.[13,14] As the POMS is used to evaluate a responder's typical mood states rather than personality traits,[15] one can assume that the observed correlation would reflect a state-dependent effect. However, because of the experimental design used in the previous study, i.e., across-subject design, we could not deny the possibility of the contribution of individual trait factors (e.g., personality traits or dispositional moods) in the results.

One solution to dissociate the state-dependent effect found in the previous study[12] from certain trait factors is examining whether PFC activity changes in correlation with his/her mood state using a within-individual design. In this study, we repeated three experiment sessions for each participant at 2-week intervals to trace the time-to-time mood fluctuations within individuals, which enabled us to identify the contribution of each participant's depressed mood state to the variations in their PFC activity independent of trait factors.

*These authors contributed equally to this work.

Address all correspondence to: Hiroki Sato, Hitachi, Ltd., Central Reseach Laboratory, 2520 Akanuma, Hatoyama, Saitama 350-0395 Japan; Tel: +81-492-96-6111; Fax: +81-492-96-5999; E-mail: hiroki.sato.ry@hitachi.com.

1083-3668/2011/16(12)/126007/7/$25.00 © 2011 SPIE

2 Materials and Methods

2.1 *Participants*

Seventeen healthy adults (12 males and 5 females; 25 to 48 years old) participated in the three experimental sessions at 2-week intervals. None of the participants had participated in our previous study.[12] This study was approved by the Ethics Committee of Hitachi, Ltd., and all participants provided written informed consent before the experiments.

2.2 *Mood Assessment*

At the beginning of each session, the participants' natural moods were assessed with a short form of the POMS,[13] which had been translated and validated for the Japanese general population.[14] While the POMS depicts sustained moods, previous studies have shown that it detects mood fluctuations within individuals.[16] Moreover, the test–retest reliability of POMS scores is not particularly high (0.65 to 0.74), suggesting that the score reflects a mood state rather than a personality trait.[15]

The participants rated 30 mood-related adjectives on a 5-point scale ranging from 0 ("not at all") to 4 ("extremely") on the basis of how they had been feeling during the past 1 week. The POMS consists of six identifiable mood factors: tension, depression, anger, vigor, fatigue, and confusion. In this study, we focused on the POMS depression score (POMS_D) because it had shown the most significant correlation with PFC activity for the verbal WM task in our previous study.[12]

2.3 *WM Tasks*

Immediately after the mood assessment, we measured the participants' PFC activity while they performed WM tasks. The tasks were presented through software (Platform of Stimuli and Tasks, developed at Hitachi's Central Research Laboratory), the same as in the previous study.[12] Each participant performed two types of WM tasks (verbal and spatial), which had an identical delayed-response paradigm. In both sessions, each task trial started with a 1500-ms presentation of the target stimuli (Target) on the PC display screen, which was followed by a delay of 7000 ms. A probe stimulus (Probe) was then presented for 2000 ms or until the participant responded. The participant responded by pressing a button on a handheld game controller connected to the PC. The system recorded the button pressed and the reaction time. In the verbal WM task, a set of two or four Japanese Hiragana characters were presented as the Target, and a Japanese Katakana character was presented as the Probe. The participants were instructed to judge whether the character presented as the Probe corresponded to any of the Target characters and then press the appropriate button. In the spatial WM task, the Target was the location of two or four white squares out of eight locations, and the Probe was the location of a white square. The participants were instructed to assess if the location of the white square presented as the Probe was identical to any of the locations of the squares presented as the Target. The intervals between the Probe onset and the following Target onset in the next trial were randomized from 16 to 24 s. Only a fixation cross was presented during the interval and delay period. In addition, a visual cue (changing the color of the fixation cross) was presented for 500 ms prior to trial onset. Auditory cues (1000- and 800-Hz pure tones of 100-ms duration) were presented at the onsets of the visual cue and Probe, respectively.

We organized the WM tasks into two sessions, one for the verbal WM task and the other for the spatial WM task, with a counterbalanced order across participants. Sixteen trials of one of the tasks were repeated in each session, and the sessions were separated by a short break (approximately 1 min). While in our previous experiment the WM task was intermingled with two additional conditions resulting in only five repetitions for each WM task, these conditions were not used in the present experiment. This modification made it possible to increase the number of repetitions for the WM task.

2.4 *OT Measurement*

The PFC activity was measured using an OT system (ETG-7100, Hitachi Medical Corporation, Japan). The system is based on a continuous wave (cw) NIRS technique.[9–11] Although other techniques such as time-resolved and frequency-domain techniques[17–19] are possibly advantageous for accurate estimation of brain tissue oxygenation and for depth-resolved analysis,[20–22] we used the cw NIRS technique because it has proved useful in previous practical studies.[23–28]

The OT system light sources were cw laser diodes with a wavelength of 695 or 830 nm. The average power of each source was 2 mW (for both wavelengths), and the two wavelength lights were irradiated on the skin through an incident optical fiber bundle (1.5-mm diameter). The signal intensities of the transmitted light were detected through a detection optical fiber bundle located 30 mm from the incident position at a sampling rate of 100 ms. We used 15 incident optical fiber bundles (sources) and 15 detection optical fiber bundles (detectors), which were arranged alternately, separated by 30 mm, in a 3×10 lattice pattern and embedded in a soft silicon holder. This resulted in a configuration with 47 measurement positions (defined as channels: chs), each corresponding to a midpoint of source-detector pair (Fig. 1). The holder was placed on each participant's forehead, and the optical fiber bundles contacted the skin on the forehead. Although we used a different system (ETG-4000, Hitachi Medical Corporation, Japan) in our previous study,[12] the basic specifications were common to both systems. The only difference between the two measurements was the width of the measurement area; the present study measured 47 chs (6 × 27 cm) using a 3×10 optode arrangement while our previous study measured 52 chs (6 × 30 cm) using a 3×11 optode arrangement.

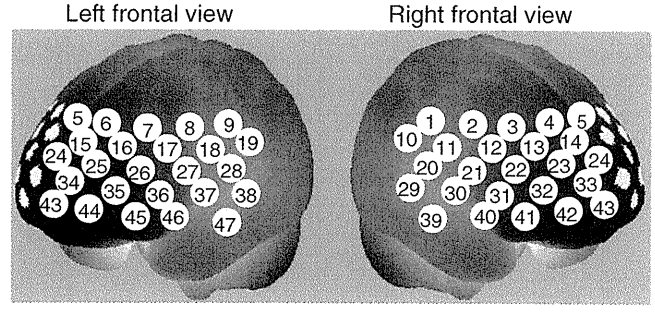

Fig. 1 Arrangement of measurement positions (47 channels) in MNI space, estimated using probabilistic registration method (Ref. 30).

The reduced width in the present study was due to a limitation in the system software. In addition, the primary activation areas identified in the previous study[12] were in the range of the measurement area of the present study.

To estimate the locations of the OT channels in the Montreal Neurological Institute (MNI) space, we used the probabilistic registration method.[29,30] Prior to the experiment, we corrected the sample data for the three-dimensional (3D) coordinates of the 30 optode locations and scalp landmarks (in accordance with the international 10 to 20 system: Fp1, Fp2, Fz, T3, T4, C3, C4) for the 11 participants. The data were recorded with a 3D-magnetic space digitizer (3D probe positioning unit for OT system, EZT-DM101, Hitachi Medical Corporation, Japan).

2.5 *Data Analysis*

Analysis was performed using the plug-in–based analysis software Platform for Optical Topography Analysis Tools (developed by Hitachi, CRL; run on MATLAB, The MathWorks, Inc., U.S.A.). First, the temporal data detected for the intensity change at each wavelength were used to calculate the products of the effective optical path length and the concentration changes of the independent hemoglobin (Hb) species ($\Delta C'_{\mathrm{oxy}}$: oxy-Hb signal, and $\Delta C'_{\mathrm{deoxy}}$: deoxy-Hb signal) for each channel on the basis of the modified Beer–Lambert law[31] as follows:

$$\Delta C'_{\mathrm{oxy}} = L \cdot \Delta C_{\mathrm{oxy}} = \frac{-\varepsilon_{\mathrm{deoxy}(\lambda 2)} \cdot \Delta A_{(\lambda 1)} + \varepsilon_{\mathrm{deoxy}}(\lambda 1) \cdot \Delta A_{(\lambda 2)}}{E}, \tag{1}$$

$$\Delta C'_{\mathrm{deoxy}} = L \cdot \Delta C_{\mathrm{deoxy}} = \frac{\varepsilon_{\mathrm{oxy}\,(\lambda 2)} \cdot \Delta A_{(\lambda 1)} - \varepsilon_{\mathrm{oxy}(\lambda 1)} \cdot \Delta A_{(\lambda 2)}}{E}, \tag{2}$$

where

$$E = \varepsilon_{\mathrm{deoxy}(\lambda 1)} \cdot \varepsilon_{\mathrm{oxy}(\lambda 2)} - \varepsilon_{\mathrm{deoxy}\,(\lambda 2)} \cdot \varepsilon_{\mathrm{oxy}\,(\lambda 1)}. \tag{3}$$

$\Delta C'_{\mathrm{oxy}}$ and $\Delta C'_{\mathrm{deoxy}}$ are expressed as the indefinite effective optical path length in the activation region (L) multiplied by the concentration change (ΔC_{oxy} and $\Delta C_{\mathrm{deoxy}}$). ΔA, $\varepsilon_{\mathrm{oxy}}$, and $\varepsilon_{\mathrm{deoxy}}$ indicate the logarithm of the intensity change in the detected light, the absorption coefficient of the oxygenated hemoglobin, and that of the deoxygenated hemoglobin, respectively, for the two wavelengths ($\lambda 1$, $\lambda 2$). We assume that the effective optical path length (L) is equal for every wavelength because accurate estimation of L is almost impossible with current techniques.[32] We used the oxy-Hb signals ($\Delta C''_{\mathrm{oxy}}$) in our analysis because we had previously observed clearer responses in these signals than in the deoxy-Hb signals.[12,33,34] To extract the task-related components from the raw oxy-Hb signals, we primarily used independent component analysis (ICA) following a published procedure.[35] Using this procedure, we reconstructed task-related oxy-Hb signals from the independent components that exceeded a criterion of 0.2 for the mean intertrial cross correlation.[35]

The time-continuous data of the oxy-Hb signals for each channel were separated into task blocks, which were defined as 25.5-s periods starting from 1.0 s before Target onset and ending 16.0 s after Probe onset, each containing a WM task trial. We removed blocks contaminated by a motion artifact, which was defined as a raw oxy-Hb signal change larger than 0.4 mM · mm over two successive samples (200-ms duration), as we did in our previous study.[12] We selected 0.4 mM · mm as the threshold level because we had found that sharp noises (putatively unphysiological signal changes) identified by a visual inspection of the data from our previous study[12] were effectively detected at this level. The remaining data were baseline corrected by linear regression based on the least squares method by using the data for the first second and the final second of each task block.

To evaluate PFC activity during the tasks, we defined the "activation period" as the 5-s period starting 5.0 s after Target onset, taking into consideration the delay in hemodynamic changes from neuronal activity mainly related to the encoding process. The mean signal changes during the activation period (x_i) were calculated for the oxy-Hb signal for each task block. Using the mean value of x_i across task blocks, we calculated within-participant z-values (converted from t-statistics) for each channel, taking intertrial variability into consideration as follows:

$$z = \frac{\overline{x}}{SD}, \tag{4}$$

where

$$\overline{x} = \frac{1}{n}\sum_{i=1}^{n} x_i, \tag{5}$$

and

$$SD = \sqrt{\frac{1}{n}\sum_{i=1}^{n}(x_i - \overline{x})^2}. \tag{6}$$

The z-values are expressed as the mean x_i [Eq. (5)] divided by the intertrial variability, which is given by the standard deviation of the x_i across task trials [Eq. (6)]. The z-values were defined as activation values (Act_V and Act_S) and represented the activation strengths for the verbal WM task (Act_V) and spatial WM task (Act_S). For the correlation analysis, we calculated the differences between successive sessions (Δ1st to 2nd and Δ2nd to 3rd) in Act_S (ΔAct_S), in Act_V (ΔAct_V), and in POMS_D (ΔPOMS_D) for each participant. These time-to-time fluctuations by individuals enabled us to identify the contribution of each participant's mood state on their PFC activity independent of trait factors. In the correlation analysis, the Spearman (rank) partial correlation with control variables of age and gender was used.

3 Results

Behavioral data (accuracy and reaction time: RT) for the WM tasks are listed in Table 1. An analysis of variance (ANOVA) with session order (1st, 2nd, and 3rd) and WM task (verbal and spatial) as within-participant factors revealed that there was no significant main effect of session order for both accuracy ($p = 0.47$) and RT ($p = 0.29$). On the other hand, a significant main effect of WM tasks was indicated for RT ($p = 0.005$), which means that RT for the verbal WM task was longer than that for the spatial WM tasks. However, the verbal WM task tended to show higher accuracy than the spatial WM task, though it was not significant ($p = 0.14$). The mean and standard deviation (SD) of POMS_D were 2.47 ± 2.67 for the 1st session, 1.88 ± 2.23 for the 2nd session, and 2.65 ± 2.91 for the 3rd session.

To examine the basic activation pattern during WM tasks, we first conducted across-participants t-test of the activation

Table 1 Mean accuracy and RT for WM tasks.

	Verbal			Spatial		
	1st	2nd	3rd	1st	2nd	3rd
Accuracy (%)	97.8	97.4	96.3	96.0	96.3	94.9
SD	4.8	5.1	7.2	7.4	7.2	9.3
RT (ms)	1250	1164	1165	1109	1122	1069
SD	208	188	263	205	261	255

values (Act_V and Act_S) for each session [Fig. 2(a)]. Channels in the bilateral dorsolateral PFC showed significantly positive values in all cases ($p < 0.05$). In particular, ch22 in the right hemisphere and ch26 in the left hemisphere consistently showed prominent activation ($p < 0.01$) for all sessions for both WM tasks [marked channels in Fig. 2(a)]. For these main activation channels, a session dependency (order effect) on the activation values was tested using the repeated-measures ANOVA with session order (1st, 2nd, and 3rd) and WM task (verbal and spatial). This analysis showed no main effect of the session order (ch22: $p = 0.96$, ch26: $p = 0.28$) with no interaction between session order and WM task (ch22: $p = 0.59$, ch26: $p = 0.76$), indicating the same activation pattern was reproduced for all sessions regardless of the WM type. The similarity of the time courses in activation signals among sessions is shown in Fig. 2(b). In addition, the main effect of WM tasks indicated no significant effect in the two channels (ch22: $p = 0.90$, ch26: $p = 0.15$).

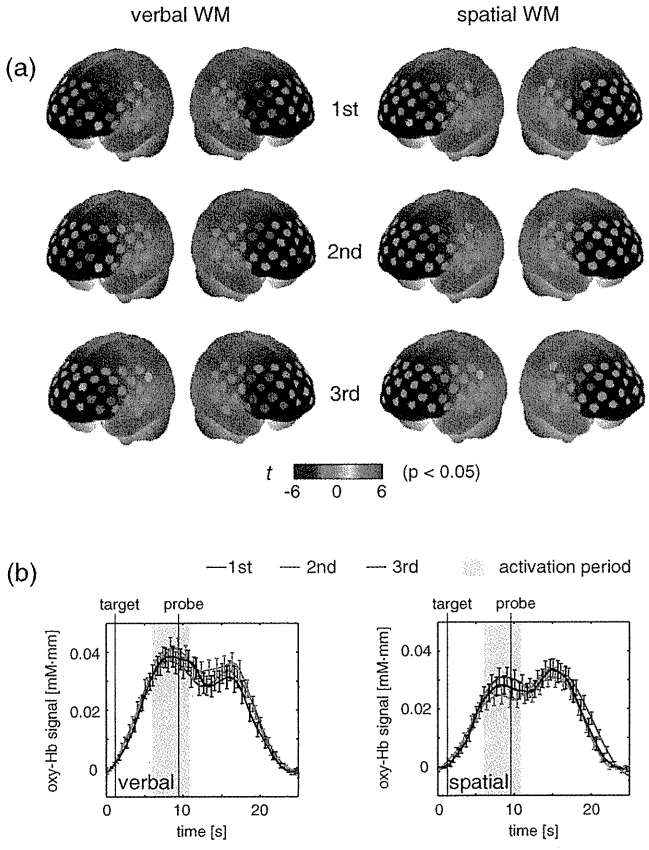

Fig. 2 Reproducibility of cortical activation for verbal and spatial WM tasks. (a) *t*-maps of activation values among participants. Channels with significant activation (determined with one-sample *t*-test against zero) are indicated with color scale shown below (two-tailed, $p < 0.05$). (b) Mean time courses of reconstructed oxy-Hb signals for representative channel (ch22 in Fig. 1). Yellow bars perpendicular to the *x*-axis indicate activation period (5-s duration). Error bars indicate standard errors across participants.

To reveal the relationship between within-individual changes in depressed mood state and PFC activation for WM tasks, we calculated the Spearman rank correlation coefficient (ρ) between ΔPOMS_D and ΔAct_V (or ΔAct_S) for each channel. The ρ-maps for Δ1st to 2nd and Δ2nd to 3rd are shown in Fig. 3(a). We regarded the channels, in which the p-values were less than 0.05 for both Δ1st to 2nd and Δ2nd to 3rd, as significantly correlated. This result indicated significantly negative correlations between ΔPOMS_D and ΔAct_V for channels mainly located in the left dorsolateral PFC (ch26 and ch35) and around the left pre-motor and supplementary motor cortex (ch8 and ch19). In contrast, the correlation coefficients between ΔAct_S and ΔPOMS_D did not reach statistical significance (the higher $p > 0.21$). These results were consistent with our previous results.[12] The distributions of ρ-values among[12] channels are shown with histograms [Fig. 3(b)] to demonstrate the discrepancy between ΔAct_V and ΔAct_S.

Figure 4 shows the negative correlation between ΔPOMS_D and ΔAct_V in the left dorsolateral PFC (ch26 and ch35), where clear WM-related activity was demonstrated (Fig. 2). The p-values for the correlation coefficients were 0.0315 and 0.0292 for Δ1st to 2nd and Δ2nd to 3rd, respectively. These p-values mean that the probability of obtaining these correlation coefficients is 0.00092 (0.0315×0.0292), which is below the corrected p-value of 0.05 for all 47 channels ($0.05/47 = 0.00106$). This indicates that decreased depressed mood score (POMS_D) is correlated with increased PFC activity for the verbal WM task (Act_V).

The within-individual fluctuations of POMS_D and Act_V (mean of ch26 and ch35) are shown in Fig. 5 for all participants, where the POMS_D is denoted on the reversed *Y*-axis. Although the sensitivities might be different, the basic change pattern for Act_V and reversed POMS_D across sessions appears to be similar in most participants.

4 Discussion

We used OT to show that fluctuations in the depressed mood state within individuals are correlated with their PFC activity during a verbal WM task. The results are consistent with those of our previous study[12] and confirm the state-dependent feature of PFC activity, which cannot be explained by the effects of certain trait differences among individuals.

The mean activation patterns for WM tasks were well reproduced, as shown in Fig. 2. The central channels of the activation were located in the dorsolateral PFC, which is consistent with other fMRI studies.[36] Moreover, the strong similarity between the activation patterns found in the present study with those found in our previous study[12] suggests that OT measurement is highly reliable for detecting cortical activity for these WM tasks. We found no main effect of session order for the PFC activity, suggesting that there was no simple order effect in our

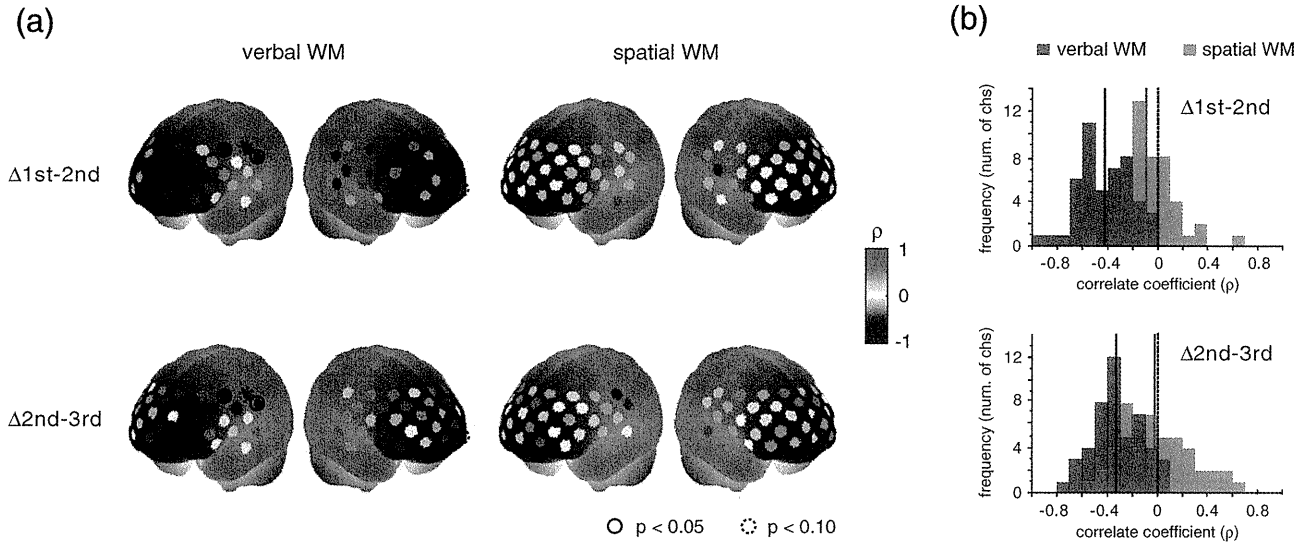

Fig. 3 Relationship between variations in depressed mood state (POMS_D) and those in activation values for verbal and spatial WM tasks (Act_V and _Act_S). (a) Statistical ρ-maps indicating correlation coefficients (Spearman ρ) between ΔPOMS_D and ΔAct_V (or ΔAct_S). Channels that showed correlation coefficients ($p < 0.05$) in both Δ1st to 2nd and Δ2nd to 3rd are marked with solid circles. In addition, channels that showed correlation coefficients ($p < 0.10$) in both Δ1st to 2nd and Δ2nd to 3rd are marked with dashed circles. (b) Histograms illustrating distributions of ρ-values for each WM task. Blue vertical line denotes median ρ-value for verbal WM task, and red vertical line denotes median ρ-value for spatial WM task among 47 channels.

measurements. In addition, the oxy-Hb signals in a representative channel demonstrated overlapped time courses among three sessions. These results support that relevant cortical activity for WM functions can be extracted using ICA.[35] Regarding differences between verbal and spatial WM tasks, the activation regions for the verbal WM task appeared to be larger than those for the spatial WM task. However, no significant main-effect of WM tasks was found in the channels that showed significant correlation coefficients between ΔPOMS_D and ΔAct_V (ch8: $p = 0.94$, ch19: $p = 0.12$, ch26: $p = 0.15$, ch35: $p = 0.07$). In addition, the behavioral data did not reveal significant differences between the two tasks in terms of difficulty. The RT for the verbal WM task was longer than that for the spatial WM tasks, which was possibly due to a difference in the task strategy, as participants showed higher accuracy for the verbal WM task than for the spatial WM task.

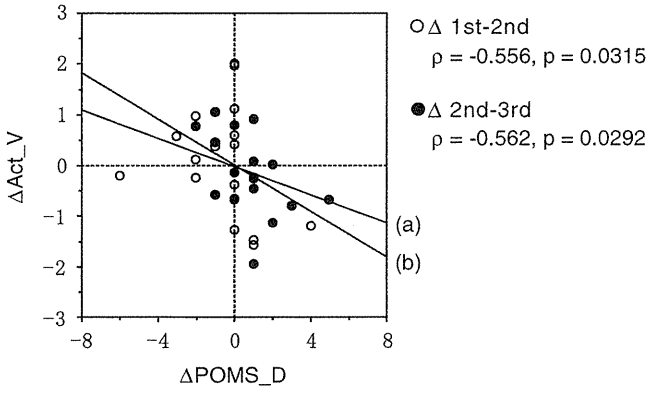

Fig. 4 Scatter plot showing relationship between ΔPOMS_D and ΔAct_V in left dorsolateral PFC (mean of ch26 and ch35). (a) Regression line of data for Δ1st to 2nd. (b) Regression line of data for Δ2nd to 3rd.

The basic activation patterns were thus similar in both WM tasks, but the correlation analysis revealed a contrast between tasks in relation to the depressed mood state (POMS_D). The negative correlation between ΔPOMS_D and ΔAct_V were well reproduced in the two independent differences between successive sessions (Δ1st to 2nd and Δ2nd to 3rd), while there were consistently no significant correlations between ΔPOMS_D and ΔAct_S. This result suggests that the PFC activity induced by a verbal WM task is selectively related to an individual's depressed mood state. In addition, the significant channels were mainly located in the left dorsolateral PFC, which is consistent with previous results.[12] Thus, we found that the interindividual variation in PFC activity during a verbal WM task[12] is not simply an indirect reflection of individual differences in trait factors; it actually reflects time-to-time fluctuations in the depressed mood state of an individual. Although the inherent limitation of transcranial NIRS requires that we consider the effect of hemodynamic changes in the extracerebral tissue, such as changes in skin blood flow,[37,38] our task paradigm did not impose intense physical or psychological demands, which could induce systemic changes. Moreover, the effect of extracerebral hemodynamic changes could not account for our finding that there is selective negative correlation between ΔPOMS_D and ΔAct_V in a localized area.

We plotted the within-individual fluctuations of POMS_D and Act_V (Fig. 5) to indicate the feasibility of using OT signals for assessing the depressed mood state of healthy participants. While Act_V apparently fluctuated in parallel with POMS_D within individuals, we could not estimate its effectiveness or validity because the depressed mood state is a psychological construct and difficult to define. To uncover new ways of using optical topography to obtain a potential state marker for an individual's mood state, we need to further clarify the interactions between the depressed mood state and PFC activity on the

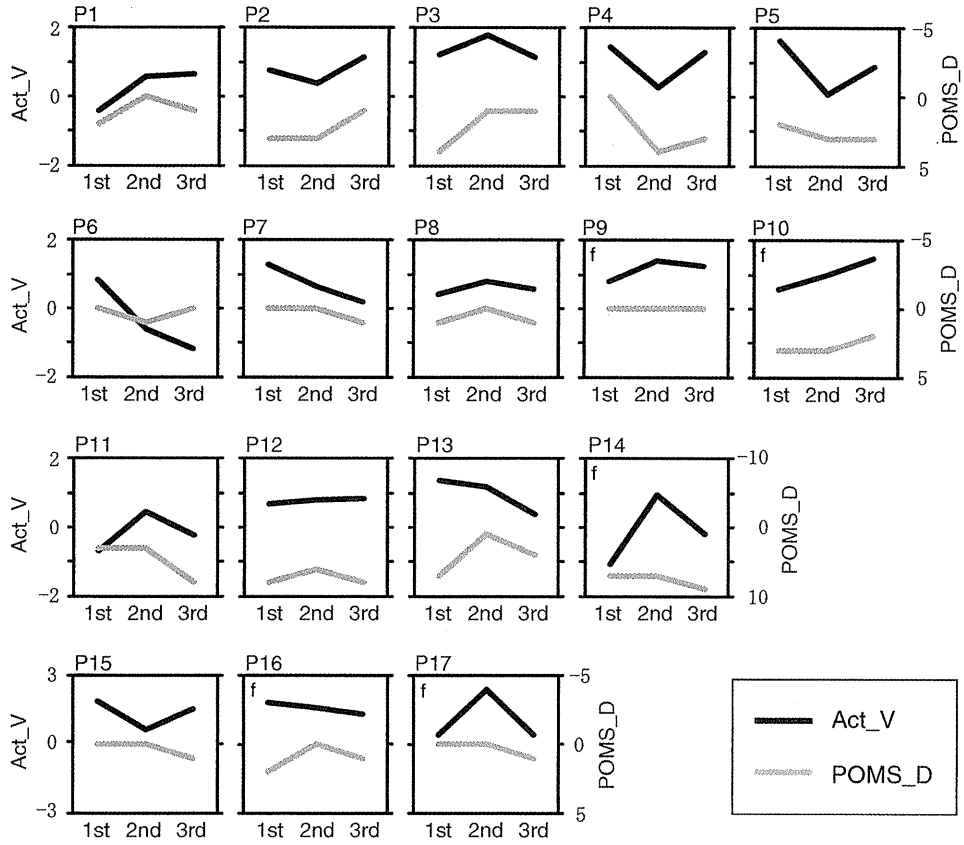

Fig. 5 Monthly fluctuations in POMS_D and Act_V (mean of ch26 and ch35) shown for every 2 weeks for all participants. Graphs with small "f" in top-left corner indicate data from females.

basis of neurophysiology, such as by using a pharmacological approach.[39–41]

5 Conclusion

We demonstrated that prefrontal cortex activity during a verbal working memory task varies depending on the participant's depressed mood state, independent of trait factors. This suggests that using optical topography to measure PFC activity during a verbal WM task can be used as a potential state marker for an individual's depressed mood state.

Acknowledgments

We thank Dr. Masashi Kiguchi, Dr. Atsushi Maki, and Dr. Kisou Kubota for their insightful comments and constructive suggestions during our discussions with them. We also thank Dr. Akiko N. Obata, Dr. Hirokazu Atsumori, Ms. Yukari Yamamoto, and Mr. Tsukasa Funane for their helpful support.

References

1. R. L. Mitchell and L. H. Phillips, "The psychological, neurochemical and functional neuroanatomical mediators of the effects of positive and negative mood on executive functions," *Neuropsychologia* **45**(4), 617–629 (2007).
2. L. Pessoa, "On the relationship between emotion and cognition," *Nat. Rev. Neurosci.* **9**(2), 148–158 (2008).
3. E. I. Bartolic, M. R. Basso, B. K. Schefft, T. Glauser, and M. Titanic-Schefft, "Effects of experimentally-induced emotional states on frontal lobe cognitive task performance," *Neuropsychologia* **37**(6), 677–683 (1999).
4. M. R. Basso, B. K. Schefft, M. D. Ris, and W. N. Dember, "Mood and global-local visual processing," *J. Int. Neuropsychol. Soc.* **2**(3), 249–255 (1996).
5. N. A. Harrison, L. Brydon, C. Walker, M. A. Gray, A. Steptoe, R. J. Dolan, and H. D. Critchley, "Neural origins of human sickness in interoceptive responses to inflammation," *Biol Psychiatry* **66**(5), 415–422 (2009).
6. S. Qin, E. J. Hermans, H. J. van Marle, J. Luo, and G. Fernandez, "Acute psychological stress reduces working memory-related activity in the dorsolateral prefrontal cortex," *Biol. Psychiatry* **66**(1), 25–32 (2009).
7. M. Suda, M. Fukuda, T. Sato, S. Iwata, M. Song, M. Kameyama, and M. Mikuni, "Subjective feeling of psychological fatigue is related to decreased reactivity in ventrolateral prefrontal cortex," *Brain Res.* **1252**, 152–160 (2009).
8. M. Suda, T. Sato, M. Kameyama, M. Ito, T. Suto, Y. Yamagishi, T. Uehara, M. Fukuda, and M. Mikuni, "Decreased cortical reactivity underlies subjective daytime light sleepiness in healthy subjects: a multichannel near-infrared spectroscopy study," *Neurosci. Res.* **60**(3), 319–326 (2008).
9. A. Maki, Y. Yamashita, Y. Ito, E. Watanabe, Y. Mayanagi, and H. Koizumi, "Spatial and temporal analysis of human motor activity using noninvasive NIR topography," *Med. Phys.* **22**(12), 1997–2005 (1995).
10. Y. Yamashita, A. Maki, Y. Ito, E. Watanabe, H. Mayanagi, and H. Koizumi, "Noninvasive near-infrared topography of human brain activity using intensity modulation spectroscopy," *Opt. Eng.* **35**, 1046–1099 (1996).
11. Y. Yamashita, A. Maki, and H. Koizumi, "Measurement system for noninvasive dynamic optical topography ," *J. Biomed. Opt.* **4**(4), 414–417 (1999).
12. R. Aoki, H. Sato, T. Katura, K. Utsugi, H. Koizumi, R. Matsuda, and A. Maki, "Relationship of negative mood with prefrontal cortex activity

during working memory tasks: An optical topography study," *Neurosci. Res.* **70**, 189–196 (2011).
13. P. M. McNair, M. Lorr, and L. F. Dropplemen, *Profile of Mood States Manual, Educational and Industrial Testing Service*, San Diego (1971).
14. K. Yokoyama, S. Araki, N. Kawakami, and T. Takeshita, "[Production of the Japanese edition of profile of mood states (POMS): assessment of reliability and validity]," *Nippon Koshu Eisei Zasshi* **37**(11), 913–918 (1990).
15. D. M. McNair and J. P. Heuchert, *Profile of Mood States Technical Update*, Multi-Health Systems, New York (2003).
16. B. G. Berger and R. W. Motl, "Exercise and mood: a selective review and synthesis of research employing the Profile of Mood States," *J. Appl. Sport Psychol.* **12**(1), 69–92 (2000).
17. A. Duncan, J. H. Meek, M. Clemence, C. E. Elwell, L. Tyszczuk, M. Cope, and D. T. Delpy, "Optical pathlength measurements on adult head, calf and forearm and the head of the newborn infant using phase resolved optical spectroscopy," *Phys. Med. Biol.* **40**(2), 295–304 (1995).
18. M. S. Patterson, B. Chance, and B. C. Wilson, "Time resolved reflectance and transmittance for the non-invasive measurement of tissue optical properties," *Appl. Opt.* **28**(12), 2331–2336 (1989).
19. M. S. Patterson, J. D. Moulton, B. C. Wilson, K. W. Berndt, and J. R. Lakowicz, "Frequency-domain reflectance for the determination of the scattering and absorption properties of tissue," *Appl. Opt.* **30**(31), 4474–4476 (1991).
20. D. Contini, A. Torricelli, A. Pifferi, L. Spinelli, F. Paglia, and R. Cubeddu, "Multi-channel time-resolved system for functional near infrared spectroscopy," *Opt. Express* **14**(12), 5418–5432 (2006).
21. M. Kacprzak, A. Liebert, P. Sawosz, N. Zolek, and R. Maniewski, "Time-resolved optical imager for assessment of cerebral oxygenation," *J. Biomed. Opt.* **12**(3), 034019 (2007).
22. H. Wabnitz, M. Moeller, A. Liebert, H. Obrig, J. Steinbrink, and R. Macdonald, "Time-resolved near-infrared spectroscopy and imaging of the adult human brain," *Adv. Exp. Med. Biol.* **662**, 143–148 (2010).
23. T. Grossmann, R. Oberecker, S. P. Koch, and A. D. Friederici, "The developmental origins of voice processing in the human brain," *Neuron* **65**(6), 852–858 (2010).
24. Y. Minagawa-Kawai, H. van der Lely, F. Ramus, Y. Sato, R. Mazuka, and E. Dupoux, "Optical brain imaging reveals general auditory and language-specific processing in early infant development," *Cereb. Cortex* **21**(2), 254–261 (2011).
25. M. Pena, A. Maki, D. Kovacic, G. Dehaene-Lambertz, H. Koizumi, F. Bouquet, and J. Mehler, "Sounds and silence: an optical topography study of language recognition at birth," *Proc. Natl. Acad. Sci. U.S.A.* **100**(20), 11702–11705 (2003).
26. H. Sato, T. Takeuchi, and K. L. Sakai, "Temporal cortex activation during speech recognition: an optical topography study," *Cognition* **73**(3), B55–B66 (1999).
27. S. Tsujimoto, T. Yamamoto, H. Kawaguchi, H. Koizumi, and T. Sawaguchi, "Prefrontal cortical activation associated with working memory in adults and preschool children: an event-related optical topography study," *Cereb. Cortex* **14**(7), 703–712 (2004).
28. E. Watanabe, A. Maki, F. Kawaguchi, K. Takashiro, Y. Yamashita, H. Koizumi, and Y. Mayanagi, "Non-invasive assessment of language dominance with near-infrared spectroscopic mapping," *Neurosci. Lett.* **256**(1), 49–52 (1998).
29. M. Okamoto and I. Dan, "Automated cortical projection of head-surface locations for transcranial functional brain mapping," *Neuroimage* **26**(1), 18–28 (2005).
30. A. K. Singh, M. Okamoto, H. Dan, V. Jurcak, and I. Dan, "Spatial registration of multichannel multi-subject fNIRS data to MNI space without MRI," *Neuroimage* **27**(4), 842–851 (2005).
31. D. T. Delpy, M. Cope, P. van der Zee, S. Arridge, S. Wray, and J. Wyatt, "Estimation of optical pathlength through tissue from direct time of flight measurement," *Phys. Med. Biol.* **33**(12), 1433–1442 (1988).
32. H. Sato, M. Kiguchi, F. Kawaguchi, and A. Maki, "Practicality of wavelength selection to improve signal-to-noise ratio in near-infrared spectroscopy," *Neuroimage* **21**(4), 1554–1562 (2004).
33. H. Sato, Y. Fuchino, M. Kiguchi, T. Katura, A. Maki, T. Yoro, and H. Koizumi, "Intersubject variability of near-infrared spectroscopy signals during sensorimotor cortex activation," *J. Biomed. Opt.* **10**, 044001 (2005).
34. H. Sato, M. Kiguchi, A. Maki, Y. Fuchino, A. Obata, T. Yoro, and H. Koizumi, "Within-subject reproducibility of near-infrared spectroscopy signals in sensorimotor activation after 6 months," *J. Biomed. Opt.* **11**(1), 014021 (2006).
35. T. Katura, H. Sato, Y. Fuchino, T. Yoshida, H. Atsumori, M. Kiguchi, A. Maki, M. Abe, and N. Tanaka, "Extracting task-related activation components from optical topography measurement using independent components analysis," *J. Biomed. Opt.* **13**(5), 054008 (2008).
36. E. E. Smith and J. Jonides, "Storage and executive processes in the frontal lobes," *Science* **283**(5408), 1657–1661 (1999).
37. S. Boden, H. Obrig, C. Kohncke, H. Benav, S. P. Koch, and J. Steinbrink, "The oxygenation response to functional stimulation: is there a physiological meaning to the lag between parameters?" *Neuroimage* **36**(1), 100–107 (2007).
38. T. Takahashi, Y. Takikawa, R. Kawagoe, S. Shibuya, T. Iwano, and S. Kitazawa, "Influence of skin blood flow on near-infrared spectroscopy signals measured on the forehead during a verbal fluency task," *Neuroimage* **57**(3), 991–1002 (2011).
39. F. G. Ashby, A. M. Isen, and A. U. Turken, "A neuropsychological theory of positive affect and its influence on cognition," *Psychol. Rev.* **106**(3), 529–550 (1999).
40. D. M. Barch, "Pharmacological manipulation of human working memory," *Psychopharmacology (Berlin)* **174**(1), 126–135 (2004).
41. M. Luciana, P. F. Collins, and R. A. Depue, "Opposing roles for dopamine and serotonin in the modulation of human spatial working memory functions," *Cereb. Cortex* **8**(3), 218–226 (1998).

Mol Cell Biochem
DOI 10.1007/s11010-011-0977-0

Pharmacological inhibition of HSP90 activity negatively modulates myogenic differentiation and cell survival in C2C12 cells

Akira Wagatsuma · Masataka Shiozuka · Naoki Kotake · Kawachi Takayuki · Honda Yusuke · Kunihiko Mabuchi · Ryoichi Matsuda · Shigeru Yamada

Received: 3 April 2011 / Accepted: 29 June 2011

Abstract Heat-shock protein90 (HSP90) plays an essential role in maintaining stability and activity of its clients. HSP90 is involved in cell differentiation and survival in a variety of cell types. To elucidate the possible role of HSP90 in myogenic differentiation and cell survival, we examined the time course of changes in the expression of myogenic regulatory factors, intracellular signaling molecules, and anti-/pro-apoptotic factors when C2C12 cells were cultured in differentiation condition in the presence of a HSP90-specific inhibitor, geldanamycin. Furthermore, we examined the effects of geldanamycin on muscle regeneration in vivo. Our results showed that geldanamycin inhibited myogenic differentiation with decreased expression of MyoD, myogenin and reduced phosphorylation levels of Akt1. Geldanamycin had little effect on the phosphorylation levels of p38MAPK and ERK1/2 but reduced the phosphorylation levels of JNK. Along with myogenic differentiation, geldanamycin increased apoptotic nuclei with decreased expression of Bcl-2. The skeletal muscles forced to regenerate in the presence of geldanamycin were of poor repair with small regenerating myofibers and increased connective tissues. Together, our findings suggest that HSP90 may modulate myogenic differentiation and may be involved in cell survival.

Keywords Apoptosis · HSP90 · JNK · Myogenic differentiation · Survival

A. Wagatsuma (✉) · M. Shiozuka · K. Takayuki · H. Yusuke · R. Matsuda
Graduate School of Arts and Sciences, The University of Tokyo, Tokyo, Japan
e-mail: wagatsuma1969@yahoo.co.jp

A. Wagatsuma · K. Mabuchi
Graduate School of Information Science and Technology, The University of Tokyo, Tokyo, Japan

N. Kotake
Department of Fisheries Distribution and Management, National Fisheries University, Yamaguchi, Japan

S. Yamada
Department of Food and Health Sciences, Jissen Women's University, Tokyo, Japan

Introduction

Heat-shock proteins (HSPs) are highly conserved set of cellular proteins that are quickly induced by stressful stimuli [1] to assist in the maintenance of cellular integrity and viability [2]. Under physiological conditions, HSP90 dynamically interacts with a diverse but highly select set of inherently unstable client proteins, including steroid hormone receptors, kinases, and transcription factors [3]. The HSP90 protein acts as molecular chaperone that regulates the cellular stress response by maintaining the conformation, stability, and function of client proteins [4].

Several lines of evidence suggest important roles for HSP90 in muscle physiology, such as myofibril assembly [5], somite development [6], muscle fiber lineages [7], and myogenic differentiation [8]. Yun et al. has been, for the first time, reported that myotube formation is blocked when C2C12 cells are treated with HSP90-specific inhibitor, geldanamycin [8]. However, since their study is based on qualitative data, it is arguable to what extent pharmacological inhibition of HSP90 activity suppresses myogenic differentiation. Geldanamycin specifically interferes with this association by occupying the ATP-binding pocket of HSP90 and dissociates client proteins from the chaperone, which results in their degradation by the ubiquitin-dependent

Published online: 08 July 2011

proteasome pathway [9]. Geldanamycin causes depletion of ErbB2, Akt, and Fyn, protein kinases [8] whose functions are required for myogenic differentiation [10] and for the survival of myoblasts and myofibers [11–13]. Geldanamycin also appears to attenuate mitogen-activated protein kinase (MAPK) signaling pathways, which control key cellular functions, including proliferation, differentiation, and survival [14]. Three distinct subgroups of MAPK pathways can be distinguished in mammalian cells: p38 mitogen-activated protein kinases (p38MAPK), extracellular signal-regulated kinase 1/2 (ERK1/2), c-Jun NH(2)-terminal kinase 1/2/3 (JNK1/2/3). Destabilization of Raf-1 by geldanamycin leads to disruption of the Raf-1–MEK–ERK1/2 signaling pathway in NIH 3T3 cells [15]. Geldanamycin abolishes TNFα-mediated activation of JNK in MCF-7 cells [16] and inhibits activation of p38MAPK in NRK-52E cells [17]. Even though MAPK signaling pathways are involved in myogenic differentiation [18–20], it remains to be elucidated whether geldanamycin-mediated inhibition of HSP90 activity has an impact on MAPK pathways in myogenic cells.

Geldanamycin has shown to induce apoptotic cell death in a variety of cell types. For example, when incubating with geldanamycin, apoptotic cell death is induced in PC12 cells [21]. Geldanamycin causes dissociation of HSP90-Bcl-2, initiating the release of cytochrome *c* from mitochondria and subsequently increasing the activity of caspases, resulting apoptosis in mast cells [22]. Although it has been reported that apoptotic cell death occurs in geldanamycin-treated myogenic cells [8], there are not yet sufficient data to elucidate the effect of geldanamycin on the occurrence of apoptosis of myogenic cells.

Here, we report that pharmacological inhibition of HSP90 activity using geldanamycin suppresses myogenic differentiation with decreased expression of MyoD and myogenin and reduced phosphorylation levels of Akt1 and JNK. Along with myogenic differentiation, geldanamycin causes apoptosis with decreased expression of Bcl-2. Our results suggest that HSP90 may be necessary for regulating myogenic differentiation and cell survival through its ability to control the multiple HSP90-dependent signaling pathways.

Materials & methods

Culture of mouse myogenic cell line

C2C12 myogenic cells [23] were maintained in growth medium comprising Dulbecco's minimum essential medium (DMEM) (GIBCO BRL, LifeTechnologies Inc., Grand Island, NY) containing 20% fetal bovine serum (FBS) (Equitec-Bio, Inc., Kerrville, TX), 4 mM L-glutamine, 100 U/ml penicillin, and 100 μg/ml streptomycin (Sigma-Aldrich, Inc. St. Louis, MO) at 37°C in 5% CO_2 and 95% air. Cells were seeded on a tissue culture dish in growth medium, and 24 h later, the medium was replaced with differentiation medium consisting of DMEM supplemented with 5% horse serum (HyClone Laboratories, Inc., Logan, UT). The cells approached 70-80% confluency in growth medium (day 0) and maintained in differentiation medium (24-96 h). The cells cultured in differentiation medium were treated with dimethylsulfoxide (DMSO) or 20 nM geldanamycin (Enzo Life Sciences International, Inc., Plymouth Meeting, PA) for 24–96 h as indicated in the legend to the figures. The medium was changed every 24 h. Geldanamycin derivative, 17-(Allylamino)-17-desmethoxygeldanamycin (17-AAG) (Enzo Life Sciences Inc., Faimingdale, NY) was also used as indicated in the legend to the figures.

Animal care

Male 4-week-old C57BL/6 J (B6) mice were used and were housed in the animal facility under a 12-h light/12-h dark cycle at room temperature (23 ± 2°C) and 55 ± 5% humidity. The mice were maintained on a diet of CE-2 rodent chow (Clea Japan, Meguro, Tokyo) and given water *ad libitum*. The mice were procured after approval for the present study from The University of Tokyo Animal Ethics Committee.

Induction of muscle degeneration/regeneration

Muscle degeneration/regeneration was induced as previously described [24]. Glycerol (100 μl of 50% vol/vol) was injected in three injection sites of gastrocnemius muscle. This model provokes hypercontraction of myofibers, degeneration, and necrosis of myofibers within 24 h after the injection and shows subsequent regeneration of myofibers between 7 and 14 days after the injection. The gastrocnemius muscles were isolated at various time points after muscle injury. To inhibit the activity of HSP90, 50 μl of treatment (178 μM) or DMSO was introduced into the muscle surrounding the injury site by direct intramuscular injection at day 1, 3, 5, and 7 after the initial injury. The gastrocnemius muscles were isolated at day 10 for histochemical analysis. All procedures in the animal experiments were performed in accordance with the guidelines presented in the Guiding Principles for the Care and Use of Animals in the Field of Physiological Sciences, published by the Physiological Society of Japan.

Creatine phosphokinase (CPK) activity assay

Cells were cultured as described above. Cells were washed twice with phosphate-buffered saline (PBS) and then